

# First principle calculations of electronic and magnetic properties of Mn-doped CdS (zinc blende): a theoretical study

NISAR AHMED<sup>1,\*</sup>, AZEEM NABI<sup>2</sup>, JAWAD NISAR<sup>1</sup>, MUHAMMAD TARIQ<sup>2</sup>, MUHAMMAD ARSHAD JAVID<sup>2</sup>, M. H. NASIM<sup>1</sup>

<sup>1</sup>Pakistan Institute of Engineering and Applied Sciences, Islamabad, Pakistan

<sup>2</sup>University of Gujrat, Gujrat, Pakistan

The electronic structure and magnetic properties of Mn doped zinc blende cadmium sulfide  $\text{Cd}_{1-x}\text{Mn}_x\text{S}$  ( $x = 6.25\%$ ) have been studied using spin-polarized density functional theory within the framework of Generalized Gradient Approximation (GGA), its further corrections including Hubbard U interactions (GGA + U) and a model for exchange and correlation potential Tran Blaha modified Becke-Johnson (TB-mBJ). Ferromagnetic interactions have been observed between Mn atoms via S atom due to strong p-d hybridization. The magnetic moments on Mn and its neighboring atoms have also been studied in detail using different charge analysis techniques. It has been observed that p-d hybridization reduced the value of local magnetic moment of Mn in comparison to its free space charge value and produced small local magnetic moments on the nonmagnetic S and Cd host sites. The magnetocrystalline anisotropy in [1 0 0] and [1 1 1] directions as well as exchange splitting parameters  $N_{0\alpha}$  and  $N_{0\beta}$  have been analyzed to confirm that ferromagnetism exists. We conclude that the ferromagnetic phase in Mn-doped CdS is not stable in “near” configuration but it is stable for “far” configuration. Mn doped CdS is a p-type semiconductor and the d-states at the top of the valence band edge give a very useful material for photoluminescence and magneto-optical devices.

Keywords: *First principle calculations; Hubbard U; TB-mBJ; magnetocrystalline anisotropy*

## 1. Introduction

Room temperature diluted semiconductors are very promising materials for optoelectronics and spintronics [1]. Cadmium sulfide is also extremely photosensitive in the entire range of spectrum, from infrared to ultraviolet, with direct band gap of 2.42 eV at room temperature [2]. So, it is an attractive semiconductor in the field of photoconductive, photovoltaic or optoelectronic materials. CdS powder is used in synthesis of light emitting sources (green region), solar panels, photocells [2], laser screen materials, projection color TVs, nuclear radiation detectors [3–5], thin film transistors, optical detectors, window layer in various solar-cell configurations, photocatalysts, nonlinear optical materials, magneto-optical and non-volatile memories [6, 7].

Doping of transition metals (TMs) in nonmagnetic CdS is very important to make this material multifunctional and to achieve the desired properties [8]. Many research groups are working on II-VI semiconductors [9–11]. Sato et al. [9] has studied the effect of dopants (Fe, Co, Ni, V and Cr) in ZnS, ZnSe and ZnTe and ZnO based DMS. Liu et al. [10] considered Cu-doped CdS system and explained the half metallic ferromagnetic character. Ma et al. [12] investigated the magnetic properties of non-transition metal/element, like Be, B, C, N, O, and F-doped CdS, explained the magnetic coupling by p-p interaction involving holes. Yang et al. [13] examined the long range p-d exchange coupling interaction in Pd doped CdS. Nazir et al. [15] examined the effects of contracting the unit cell of ZnS and CdS compounds by doping with Cr, up to 6 % and 8 %, respectively, and change in half metallicity. Kumar et al. [16] analyzed the Mn-CdS sheet with 16 atom

\*E-mail: nisarbinwali@gmail.com

supercell. Rantala *et al.* [17] investigated the atomic geometry and calculated the electronic structure of wurtzite CdS using two different self-consistent ab initio LDA methods. Nabi [18] investigated electronic and magnetic properties of Mn doped CdS in wurtzite phase, using ab-initio calculations based on LDA, GGA and LDA + U exchange and correlation functionals. Moreover, Mn doped CdS is a very good photo-luminance compound due to d-states at the top of the valence band and intra-d shell transitions.

In this work, the electronic structure and magnetic properties of  $\text{Cd}_{1-x}\text{Mn}_x\text{S}$  ( $x = 6.25\%$ ) are studied using spin-polarized density functional theory within the framework of Generalized Gradient Approximation (GGA), its extension via on-site Hubbard U interactions (GGA + U) and a model for exchange and correlation potential Tran modified Becke-Johnson (TB-mBJ). The GGA-PBE with Hubbard correction term,  $U = 2.7$  eV on d-states of Mn and TB-mBJ calculations are performed. The main focus of this work is an electronic band gap, p-d hybridization and magnetocrystalline anisotropy (MCA) of Mn atoms in CdS. The literature survey indicates that no consistent research work has been reported yet for doping of Mn in zinc blende phase of CdS. The results calculated in this work are very interesting and significant for exploring the properties of the material for applications in spintronics and optoelectronics devices.

## 2. Experimental

In this work, all calculations are performed using density functional theory (DFT) as implemented in the Amsterdam density functional (ADF) program [19]. The Perdew Burke Ernzerhof (PBE) exchange correlation functional is employed within the generalized gradient approximation (GGA) and the Hubbard term is added (GGA + U). TB-mBJ functional is also used for correct band gap prediction. The GGA + U functional is used to study the magnetocrystalline anisotropy (MCA) along [1 0 0] and [1 1 1] directions. We have simulated CdS (zincblende)

by  $2 \times 2 \times 1$  supercell with the initial lattice constant  $a = b = c = 5.82 \text{ \AA}$  [20]. Two Mn atoms are added at Cd cation sites in 32-atom supercell to study the electronic structure and magnetic properties of this Mn-CdS system. In these calculations, Cd ( $5s^24d^{10}$ ), S ( $3s^23p^4$ ) and Mn ( $3d^54s^2$ ) states have been considered as valence, whereas the rest of states are considered as frozen core states. The Slater type basis sets consisting of triple zeta with spin-polarized wave functions are used for all atoms in the system. A k-point grid  $5 \times 5 \times 5$  Monkhorst-Pack mesh with relativistic effects is used for all calculations. During the relaxation of internal atomic positions, the criterion for energy convergence, gradient convergence and step convergence are fixed at  $10^{-5}$  eV,  $10^{-4}$  eV/Å and  $10^{-3}$  eV values, correspondingly. All atomic positions have been relaxed during these calculations. When the structure is fully relaxed, the values of bond lengths are found to be as follows: Cd-S it is  $2.64 \text{ \AA}$ , for Mn-Cd it is  $4.14 \text{ \AA}$  and for Mn-S it is  $2.19 \text{ \AA}$ . The electro-negativity (Pauling scale) difference for Cd(1.7)-S(2.5) bond is,  $-0.8$ , less than for Mn(1.6)-S(2.5) bond,  $-0.9$ , hence the bond length is shorter for Mn-S than Cd-S.

## 3. Results and discussions

### 3.1. Electronic properties

We have studied the cationic Mn doping in CdS to understand the effect of Mn doping on the electronic and magnetic properties of pure CdS. To study the magnetic coupling of Mn dopants, we have substituted two of Cd atoms of the 32 atom supercell with Mn which corresponds to the Mn doping concentration of 6.25 %. Crystal structure of Mn doped CdS is shown in Fig. 1.

The formation energy of this doping is defined as the energy needed to introduce such impurity in bulk CdS and can be calculated by:

$$E_f = E_T(\text{Mn-CdS}) - E_T(\text{CdS}) + n\mu_{\text{Cd}} - n\mu_{\text{Mn}} \quad (1)$$

where  $E_T(\text{Mn-CdS})$  and  $E_T(\text{CdS})$  are the total energies of doped and pure CdS, respectively. The term  $n$  is the number of doping atoms.  $\mu_{\text{Cd}}$  and  $\mu_{\text{Mn}}$  are

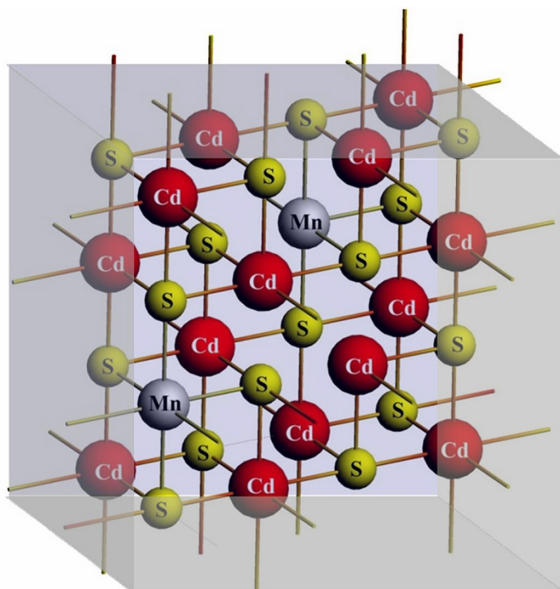


Fig. 1. Crystal structure of Mn:CdS.

the atomic potentials of Cd and dopant atoms, respectively. Formation energies calculated for different configurations are given in Table 1.

Spin polarized calculations have been performed using GGA, TB-mBJ and GGA + U to study the electronic structure of the system. Electronic band gap of the material obtained using different methodologies are given in Table 2.

TB-mBJ gives the band gap value of 2.74 eV in the minority spin channel, while GGA + U gives 1.25 eV. The value of band gap obtained with GGA + U is smaller than that of GGA in spin down state. This high value of band gap obtained with GGA in spin down channel is caused by Moss-Burstein shift (MBS) which is due to self-interaction error (SIE). Mn ( $3d^5 4s^2$ ) doped in CdS shares its  $4s^2$  electrons to make bonds with two neighboring S atoms, remaining five electrons in fivefold d levels. These five electrons fill all five spin-up d-states with high spin (HS) configuration. In ZB structure, cations are under the tetrahedral crystal field and the d-states of these cations are split into  $t_{2g}$  and  $e_g$  states. The  $t_{2g}$  states lie higher in energy than the  $e_g$  states (Fig. 2). In Mn-CdS system, the bonding  $t_{2g}$ , non-bonding  $e_g$  and anti-bonding  $t_{2g}$  states all lie below the Fermi level.

The non-bonding states are present between bonding and anti-bonding states for GGA + U and TB-mBJ, while for GGA anti-bonding states lie above the Fermi-level due to SIE which is shown in Fig. 2.

Valence band edges are generated due to hybridization between S-3p and Mn-3d (spin up) states, whereas the conduction band edges are the outcome of Cd-5s spin down states. The calculated difference between  $e_g$  and  $t_{2g}$  states for GGA, GGA + U and TB-mBJ are 1.29 eV, 0.51 eV and 1.53 eV (Table 3) [22].

The difference between  $e_g$  and  $t_{2g}$  is responsible for d-d intershell transitions. GGA cannot give an accurate physical nature of strongly correlated electrons due to SIE and shows that the material is half metallic. In order to overcome this error, we have used GGA + U which shows that the material is not half metallic but it has some band gap in both spin channels (Fig. 3).

The majority spin channels show half metallic character while the minority spin channels show some shift of Moss-Burstein type as in case of GGA and there is a band gap of 1.21 eV. The band gap energies in both majority and minority spins changed their values from 0.00 eV to 0.30 eV and 1.35 eV to 1.25 eV for GGA and GGA + U, respectively [23]. In this study, GGA and GGA + U still underestimate the band gap. In order to overcome this discrepancy, different methods have been developed to predict accurate electronic and spectroscopic properties with improved computational efficiency using standard DFT.

We have observed that GGA and GGA + U do not give the accurate picture of  $e_g$  and  $t_{2g}$  states present inside the band gap [24, 25] so this problem has been overcome by using TB-mBJ functional. Tran et al. [26] have modified Becke-Johnson (mBJ) potential to develop a semi-local exchange and correlation functional. Although it is not a significant hybrid functional but it has improved prediction accuracy of band gaps for a variety of semiconductors with d or f orbitals, oxides, insulators, rare gas solids and lithium halides, as reported in the literature [26]. The TB-mBJ gives very accurate picture of  $e_g$  and  $t_{2g}$  states present

Table 1. Energy difference ( $\Delta E = E^{\text{AFM}} - E^{\text{FM}}$ ) between antiferromagnetic and ferromagnetic alignment and total magnetic moment for bulk Mn-CdS using GGA + U ( $U_{\text{eff}} = 2.7$  eV).

$d_{\text{Mn-Mn}}$ [Å]	$\Delta E$ [eV]	$\Delta E$ [eV]	Coupling	energy of formation
3.843	-0.2338	-1.440	AFM	9.35
5.800	0.1601	-0.603	FM	6.71
7.030	-0.1203	0.182	FM	6.78

Table 2. Band gap and p-d hybridization of Mn-doped CdS with different functionals.

	GGA	GGA + U	TB-mBJ	Others
Band gap (spin up) [eV]	0.00	0.30	0.75	1.0 <sup>a</sup>
Band gap (spin down) [eV]	1.45	1.25	2.74	
$\Delta_x(\text{pd})$ [eV]	-1.20	-0.41	-1.57	

<sup>a</sup>[16, 20]

Table 3. The calculated difference between  $e_g$  and  $t_{2g}$  states for GGA, GGA + U and TB-mBJ.

	GGA [eV]	GGA + U [eV]	TB-mBJ [eV]
$e_g$	-6.97	-6.53	-5.45
$t_{2g}$	-5.68	-6.02	-3.92
$e_g - t_{2g}$	1.29	0.51	1.53

inside the band gap as depicted in Fig. 4. Due to crystal field splitting,  $e_g$  states lie lower in energy at  $-5.45$  eV and  $t_{2g}$  lie at  $-3.92$  eV, i.e. a slightly higher energy. However, the difference between  $e_g$  and  $t_{2g}$  states for TB-mBJ (1.53 eV) is greater than the calculated by GGA (1.29 eV). The comparison of DOSs shows that TB-mBJ improves the accuracy of band gap estimation and we can clearly see two bands IB-I ( $t_{2g}$ ) and IB-II ( $e_g$ ) appearing at the top of valance band maxima. These two bands are responsible for photoluminescence properties due to transitions between these states. The difference between  $e_g$  and  $t_{2g}$  states is given in Table 3 with the value for TB-mBJ being 1.53 eV, close to experimental value [22].

### 3.2. Magnetic properties

Undoped CdS is non-magnetic but on doping Mn, the total magnetic moment in CdS comes from Mn atoms and small contribution of Cd and S atoms. The magnetic moments on the nearest

neighbors of Mn atoms are induced due to p-d hybridization between S-3p and Mn-3d states. Magnetic moment on Mn atoms and their neighboring atoms are evaluated using different analysis techniques. These induced magnetic moments on Mn atoms are parallel to those on both Cd and S, which are given in Table 4.

In Table 4, the magnetic moment on Mn is calculated by using different exchange and correlation functionals GGA, GGA + U and TB-mBJ using different charge analysis techniques like Mullikan population [31], Hirschfield [32] and Voronoi Deformation Density (VDD) methods [33].

It indicates that with increasing the value of U, Mn-3d states shift apart from the Fermi level, which means that the amount of p-d hybridization decreases with increasing value of U. The nature of the sulfur 3p orbital is more complex, so weaker p-d hybridization in sulfides is found [27]. As the U value increases, the magnetic moment on Mn increases and induced values of magnetic moments on Cd and S decrease. The magnetic moment on Mn ion varies from  $3.74 \mu_B$  (GGA) to  $4.21 \mu_B$  (GGA + U).

A large amount of hybridization can be seen at the valance band ( $-2.05$  eV) using TB-mBJ between Mn-3d and S-3p states, which reduces the magnetic moment of TM from its free space value of  $5.0 \mu_B$  to  $4.21 \mu_B$ . The total energy of Mn-doped

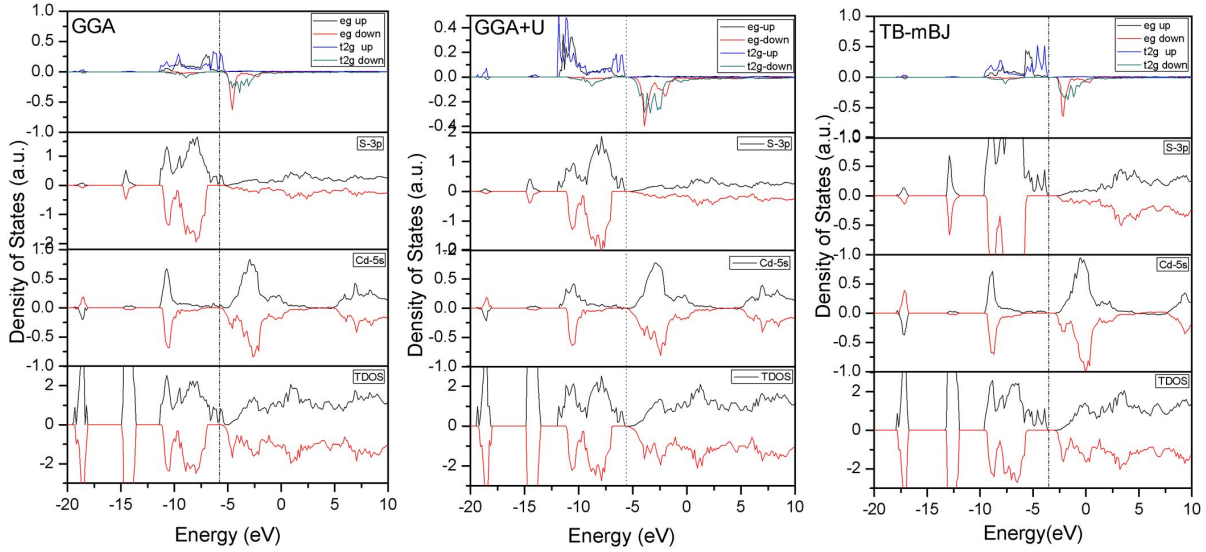


Fig. 2. Total and partial density of states for Mn-doped CdS obtained using GGA, GGA + U and TB-mBJ calculations.

Table 4. Magnetic moment ( $\mu_B$ ) on Mn atom obtained with different charge analysis techniques. MKP – Mulliken Population<sup>b</sup>, HFA – Hirshfeld charge analysis<sup>c</sup>, VOC – Voronoi charges<sup>d</sup>.

Cd <sub>14</sub> Mn <sub>2</sub> S <sub>16</sub>	Cd			S			Mn			Others
	MKP	HFA	VOC	MKP	HFA	VOC	MKP	HFA	VOC	
GGA	0.092	0.098	0.099	0.013	0.022	0.021	4.160	3.740	3.930	Mn = 4.29 <sup>a</sup>
GGA + U	0.062	0.060	0.034	0.007	0.013	0.012	4.745	4.212	4.434	Cd = 0.024 <sup>a</sup>
TB-mBJ	0.043	0.036	0.034	0.004	0.019	0.017	4.139	4.216	3.945	S = 0.051 <sup>a</sup>

<sup>a</sup>[14], <sup>b</sup>[30], <sup>c</sup>[31], <sup>d</sup>[32].

CdS is lowered because of this negative p-d coupling between Mn-3d and S-3p, which stabilizes the system in magnetic-order structure [28].

Ferromagnetic and anti-ferromagnetic (with spin flip of one of Mn atoms) calculations have been performed. Ferromagnetic configuration is stable in case of 'far' distance between two Mn atoms (5.800 Å and 7.030 Å) but anti-ferromagnetic configuration is stable in case of 'near' distance (3.843 Å). The results obtained with GGA + U functional for ferromagnetic and anti-ferromagnetic magnetic ground states are given in Table 1.

The reason for AFM order to be more stable is super-exchange interactions [9]; the e levels of one Mn<sub>1</sub> atom with majority spin couple

with the e levels of another Mn<sub>2</sub> atom with the opposite spin and result in some energy gain as shown in Fig. 5b. Moreover, super-exchange interactions are dominant over the double exchange interactions taking place between two Mn atoms and these interactions support AFM ground state. At 3.843 Å there is a very weak AFM ground state due to super-exchange interactions [27]. For FM coupling between Mn atoms, since two levels with the same spin are fully occupied, one e (Mn<sub>1</sub>) level is pushed up and other e (Mn<sub>2</sub>) level is pushed down with no energy gain as shown in Fig. 5a. Our calculations show that the material is more stable in FM ground state.

We have further calculated the value of spin-exchange splitting energy  $\Delta_x d$  from the band

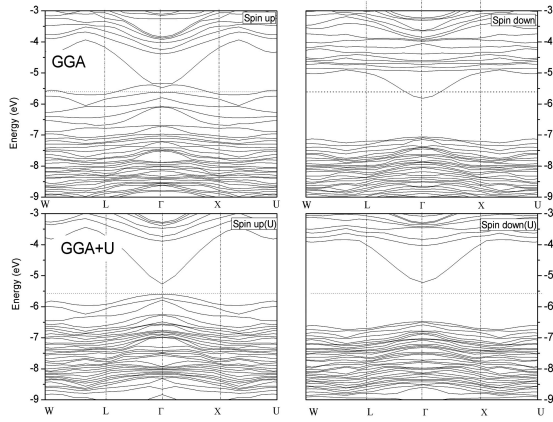


Fig. 3. Spin-dependent band structure of  $\text{Cd}_{1-x}\text{Mn}_x\text{S}$  ( $x = 6.25\%$ ) obtained with GGA and GGA + U.

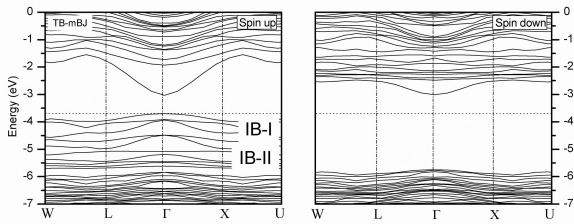


Fig. 4. Spin-dependent band structure of  $\text{Cd}_{1-x}\text{Mn}_x\text{S}$  with TB-mBJ.

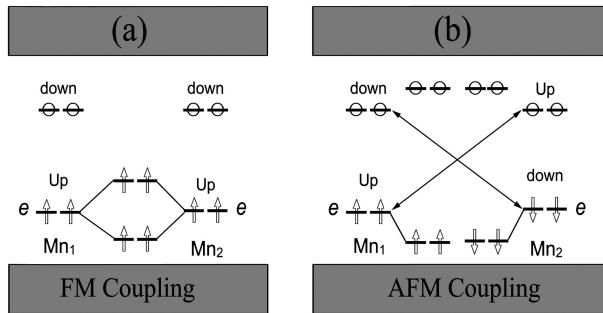


Fig. 5. Schematic view of (a) FM coupling and (b) AFM coupling between two Mn atoms.

structure diagram, which is defined as the separation between the corresponding spin-up and spin-down peaks. We have discussed the p-d exchange splitting,  $\Delta_x^v(\text{pd}) = E_v^\downarrow - E_v^\uparrow$ ,  $\Delta_x^c(\text{pd}) = E_c^\downarrow - E_c^\uparrow$  and the values of exchange parameters  $N_{o\alpha}$  and  $N_{o\beta}$ , [28], which are defined as:

$$N_{o\alpha} = \frac{\Delta E_c}{x\langle s \rangle}, \quad N_{o\beta} = \frac{\Delta E_v}{x\langle s \rangle} \quad (2)$$

where  $\Delta E_c$  and  $\Delta E_v$  are band edge splitting of conduction band and valence band,  $x\langle s \rangle$  is one half magnetization per TM atom and all these computed values are listed in Table 5.

Table 5. Exchange splitting constants Mn-CdS.

Mn-CdS	GGA	GGA + U	TB-mBJ
$\Delta_x^c d$	-0.23	-0.05	0.038
$\Delta_x^v(\text{pd})$	-1.446	-0.87	-2.05
$N_{o\alpha}$	-0.767	-0.167	0.12
$N_{o\beta}$	-4.82	-2.90	-6.83

The value of  $\Delta_x^v(\text{pd})$  is negative for Mn-CdS which means that the effective potential for minority spin is more attractive than that of majority spin for this system. The value of  $\Delta_x^c d$  is negative for GGA and GGA + U while positive for TB-mBJ. We have calculated these exchange parameters at low concentration (6.25 %) but they were previously calculated at very high concentration (25 %) of Mn in CdS [15]. Moreover, the magnetocrystalline anisotropy (MCA) [30] has been analyzed to study ferromagnetism in Mn-CdS. MCA is a direction dependent property of materials. In body centered cubic crystal, easy axis is along one [1 0 0] and [1 1 1] is hard axis. We have performed some more calculations in [1 0 0] and [1 1 1] directions by using slabs. The magnetocrystalline anisotropic energy (MAE) arises due to spin orbital coupling and we have used force theorem to calculate the MAE. The MCA is defined as the energy difference between two states with the magnetization pointing along the easy axis and hard axis  $\Delta E = E[100] - E[111]$  and the value of  $\Delta E$  in our system is 0.9 meV at the specific concentration. The results of exchange splitting and MCA confirm the magnetic nature of the material.

## 4. Conclusions

In this article, the structural, electronic and magnetic properties of Mn-doped ZB CdS are explored using GGA, GGA + U and TB-mBJ. Some non-bonding and anti-bonding states caused by the doping of Mn, which are responsible for photoluminescence in Mn-CdS, are produced at

the top of valence band. The results obtained with GGA and GGA + U do not give accurate picture of these (Mn-3d) states present inside the band gap, however, TB-mBJ gives a clear picture of these states. We have also performed a systematic study on magnetic interactions between Mn ions in Mn-doped CdS. Ferromagnetic stability has been found for different distances between adjacent Mn atoms in case of 'far' configuration while anti-ferromagnetism is favorable in case of 'near' configuration. Moreover, TB-mBJ overestimates the magnetic properties so we have used GGA + U functional to calculate the magnetic moments, MCA and ferro/anti-ferromagnetic ground states. The value of magnetic moment has been found to be  $4.21 \mu_B$  and the magnetism comes essentially from the d-states of Mn impurity atoms. The value of magnetic moment on Mn-atom increases with increasing value of  $U_{\text{eff}}$  and p-d hybridization decreases. It is also observed that p-d hybridization reduces the local magnetic moment of Mn from its free space charge value and produces small local magnetic moments on the non-magnetic Cd and S host sites which align parallel to Mn atom, which gives birth to permanent magnets. The MCA and exchange splitting constants  $N_{\alpha}$  and  $N_{\beta}$  confirm that ferromagnetism exists in Mn-CdS and hence, the material is useful for magneto-optical devices.

## References

- [1] SALIMIAN S., SHAYESTEH S.F., *J. Supercond. Nov. Magn.*, 6 (2012), 2009.
- [2] ZHANG C., YAN S., *J. Appl. Phys.*, 4 (2010), 043913.
- [3] HASANZADEH J., YESTEH S.F., *Opt. Appl.*, 41 (2011), 921.
- [4] RUXANDRA V., ANTOHE S., *J. Appl. Phys.*, 2 (1998), 727.
- [5] CHU H.-Y., LIU Z.-X., QIU G.-L., KONG D.-G., WU S.-X., LI Y.-C., DU Z.-L., *Chinese Phys. B*, 17 (2008), 2478.
- [6] YANG Z., GAO D., ZHU Z., ZHANG J., SHI Z., ZHANG Z., XUE D., *Nanoscale Res. Lett.*, 1 (2013), 17.
- [7] CHANDRAMOHAN S., KANJILAL A., STRACHE T., TRIPATHI J.K., SARANGI S.N., SATHYAMOORTHY R., SOM T., *Appl. Surf. Sci.*, 2 (2009), 465.
- [8] DELIKANLI S., HE S., QIN Y., ZHANG P., ZENG H., ZHANG H., SWIHART M., *Appl. Phys. Lett.*, 13 (2008), 132501.
- [9] SATO K., KATAYAMA-YOSHIDA H., *Semicond. Sci. Tech.*, 4 (2002) 367.
- [10] LIU M., DU Y., MA L., JING D., GUO L., *Int. J. Hydrogen Energ.*, 1 (2012), 730.
- [11] GE X., ZHANG Y., *J. Magn. Magn. Mater.*, 3 (2009), 198.
- [12] MA Y., DAI Y., HUANG B., *Comp. Mater. Sci.*, 5 (2011), 1661.
- [13] YANG Z., GAO D., XUE D., *Nanoscale Res. Lett.*, 1 (2013), 17.
- [14] NAZIR S., IKRAM N., TANVEER M., *J. Phys. Chem. A*, 20 (2009), 6022.
- [15] NAZIR S., IKRAM N., SIDDIQI S.A., SAEED Y., SHAUKAT A., RESHAK A.H., *Curr. Opin. Solid St. M.*, 1 (2010), 1.
- [16] KUMAR S., KUMAR A., AHLUWALIA P.K., *First principle study of manganese doped cadmium sulphide sheet*, in: MURLI C., BHATTACHARYYA D., GADKARI S.C. (Ed.), *AIP Conference Proceedings*, AIP, New York, 2014, p. 1732.
- [17] RANTALA T.T., RANTALA T.S., LANTTO V., VAARA J., *Surf. Sci.*, 352 (1996), 77.
- [18] NABI A., *Comp. Mater. Sci.*, A (2016), 210.
- [19] [www.scm.com](http://www.scm.com).
- [20] JI X., LI H., CHENG S., WU Z., DONG Y.X., PENGXUN YAN, *Mater. Lett.*, 17 (2011), 2776.
- [21] SALMANI E., BENYOUSSEF A., EZ-ZAHRAOUI H., SAIDI E.H., MOUNKACHI O., *Chinese Phys. B*, 10 (2012), 106601.
- [22] SRIVASTAVA P., KUMAR P., *J. Nanopart. Res.*, 10 (2011), 5077.
- [23] ZHANG C., YAN S., WANG P., ZHANG Z., *Comp. Mater. Sci.*, 4 (2008), 710.
- [24] ANISIMOV V.I., ZAAANEN J., ANDERSEN O.K., *Phys. Rev. B*, 3 (1991), 943.
- [25] PICKETT W.E., ERWIN S.C., ETHRIDGE E.C., *Phys. Rev. B*, 3 (1998), 1201.
- [26] TRAN F., BLAHA P., *Phys. Rev. Lett.*, 22 (2009), 226401.
- [27] DEV P., XUE Y., ZHANG P., *Phys. Rev. Lett.*, 11 (2008), 117204.
- [28] KACZKOWSKI J., JEZIERSKI A., *Acta Phys. Pol. A*, 5 (2009), 924.
- [29] AMARI S., MECABIH S., ABBAR B., BOUHAFS B., *J. Magn. Magn. Mater.*, 18 (2012), 2800.
- [30] DÄNE M., KIM S.K., SURH M.P., ÅBERG D., BENEDICT L.X., *J. Phys.-Condens. Mat.*, 26 (2015), 266002.
- [31] MULLIKEN R.S., *J. Chem. Phys.*, 10 (1955), 1833.
- [32] HIRSHFELD F.L., *Theoret. Chim. Acta*, 2 (1977), 129.
- [33] GUERRA C.F., HANDGRAAF J.W., BAERENDS E.J., BICKELHAUPT F.M., *J. Comput. Chem.*, 2 (2004), 189.

Received 2016-08-31

Accepted 2017-09-24